Gas-Phase Chemistry of Solid-Fuel Particle Combustion

6

Francesca Loffredo, Raymond Langer, Maximilian Hellmuth, Sanket Girhe, Anita Meraviglia, Bingjie Chen and Heinz Pitsch

Contents

Abstract

This chapter discusses kinetic modelling of the gas-phase chemistry for biomass combustion under oxy-fuel conditions. Several datasets of species mole frac-

F. Loffredo (✉) · R. Langer · M. Hellmuth · S. Girhe · A. Meraviglia · B. Chen · H. Pitsch
Institute for Combustion Technology, RWTH Aachen University, Aachen, Germany
e-mail: f.loffredo@itv.rwth-aachen.de

R. Langer
e-mail: r.langer@itv.rwth-aachen.de

M. Hellmuth
e-mail: m.hellmuth@itv.rwth-aachen.de

S. Girhe
e-mail: s.girhe@itv.rwth-aachen.de

A. Meraviglia
e-mail: a.meraviglia@itv.rwth-aachen.de

B. Chen
e-mail: b.chen@itv.rwth-aachen.de

H. Pitsch
e-mail: h.pitsch@itv.rwth-aachen.de

R. Kneer et al. (eds.), *Clean Energy Conversion*,
https://doi.org/10.1007/978-3-031-98956-8_6

tion measurements obtained from counterflow flames covering a broad range of conditions and fuels were utilised to assess the progress in detailed kinetic modelling of polycyclic aromatic hydrocarbons and to identify a detailed chemical kinetic model suitable for further investigations of solid fuel combustion under oxy-fuel conditions. The selected model was amended by a NO_x submodel and the oxidation chemistry of oxygenated and nitrogen-containing tar species, i.e. anisole, levoglucosan, propionaldehyde, ammonia, and pyridine. A multistep reduction approach provided a skeletal kinetic model for biomass gas-phase combustion with 104 species (140 species, including the NO_x submodel), which can be used to perform complex simulations at reduced computational cost. The validation of these skeletal models against experimental data representative of atmospheric high-temperature combustion under oxy-fuel conditions and in air demonstrated the models' prediction accuracy and suitability for practically relevant applications.

6.1 Introduction

Developing models that accurately predict the properties of solid fuel combustion is a considerable scientific challenge. Combustion of coal or biomass is a multiphase process comprising three main stages: devolatilisation, gas-phase combustion, and char burnout [1]. When solid fuel particles are exposed to heat, their surface temperature rises, initially causing contained water to evaporate. As the temperature increases further, the solid fuel undergoes thermal decomposition, releasing light gases and tars. This volatile matter mixes with oxygen in the surrounding environment, combusting in the gas phase, a stage that is particularly important for biomass as it involves the rapid release of most energy [1,2]. In the final stage, the remaining char is oxidised. This chapter addresses gas-phase combustion (second stage) in the form of chemical kinetic models.

In general, solid fuel combustion is a diffusion-controlled process, where the rate of combustion is dictated by the diffusion of oxygen into the flame zone. However, results from direct numerical simulations [3] show that in practical applications, premixed and non-premixed combustion may be relevant due to local extinction and re-ignition. Chemical kinetic models developed for describing oxy-fuel combustion must be able to predict such phenomena for the broad range of species observed in volatile matter. At the same time, the high computational cost of simulations, the iterative nature of the model development process, and requirements on uncertainty and richness of experimental data for model validation demand simplifications. The counterflow configuration is the simplest configuration that reflects the importance of both non-premixed combustion and Damköhler numbers. Additionally, its relatively simple geometry permits the analysis of kinetic models through numerically obtained one-dimensional similarity solutions [4], reducing the computational effort. Therefore, this work's validation and analysis of chemical kinetic models focuses on measurements in counterflow diffusion flames. These are complemented by experimental data from jet-stirred reactors (JSR) covering the premixed combustion modes.

Besides combustion phenomena, such as heat release, extinction, and re-ignition, solid fuel combustion modelling often requires quantifying pollutants, such as nitrogen oxides (NO_x) and soot. Accurate NO_x predictions can be challenging for biomass combustion because of the high content of organically bound nitrogen (N) within the molecular structure of the fuel [5]. The release of nitrogen-containing volatiles leads to potentially high NO_x emissions [6,7], necessitating the investigation of their formation pathways. Further, prediction uncertainties of soot formation and oxidation remain large and can often exceed two orders of magnitude [8]. Although accumulating evidence suggests that polycyclic aromatic hydrocarbons (PAHs) are the gaseous precursors of soot particles [8], several steps in the formation processes of this pollutant are not yet fully understood and remain an active area of research. This work assesses the progress towards quantitatively accurate predictions of these pollutants under oxy-fuel conditions. NO_x and soot formation are relatively slow processes compared to fuel oxidation. Therefore, residence time strongly impacts NO_x and soot formation. The counterflow and JSR configurations facilitate direct access to residence times, which makes it possible to mimic the conditions in technical applications and renders experimental measurements with these setups an excellent choice for investigating pollutant formation.

While predicting combustion phenomena and pollutants requires detailed models containing numerous species, considering all components of light volatiles and tars is neither feasible nor practical. Instead, the composition and properties of the actual fuel are often approximated by simplified surrogate formulations with a small number of representative components [9]. Besides various hydrocarbons, surrogate mixtures typically include oxygenated and nitrogen-containing species. Pyrolysis studies of algae, plant matter, and animal proteins identified the primary nitrogen-containing compounds in light volatiles and tar species [10,11]. Among the light volatiles, ammonia (NH_3) and hydrogen cyanide (HCN) are the predominant nitrogen-containing species [5–7]. Chemical analyses of tars revealed pyrrole (C_4H_5N), pyridine (C_5H_5N), and piperazine ($C_4H_{10}N_2$) as the main nitrogen-containing compounds [12–14]. For oxygenated species, vanillin ($C_8H_8O_3$) and anisole (A_1OCH_3) were identified as key surrogate components [13,14].

This chapter first evaluates the recent progress in modelling gas-phase chemistry for solid fuel combustion, focusing on oxy-fuel conditions (Sect. 6.2). Several data sets of species mole fraction measurements obtained within the CRC/TRR 129 and compiled from the literature are utilised to assess the progress in detailed kinetic modelling of PAHs and identify a detailed chemical kinetic model suitable for further investigations. The identified detailed model is amended by nitrogen chemistry and surrogate components relevant to biomass combustion, and subsequently reduced in a series of steps (Sect. 6.3). Concluding, a compact kinetic model is proposed for the investigation of atmospheric, high-temperature combustion under oxy-fuel conditions, which is suitable for simulating complex application cases at reduced computational costs.

6.2 Detailed Modelling of PAH Formation Under Oxy-Fuel Conditions

Over the past decade, several studies advanced the understanding of gas-phase kinetics in biomass and coal combustion under oxy-fuel conditions. Besides the C_0–C_4 core chemistry [15–19], the formation and oxidation of nitrogen-containing and oxygenated tars, such as pyrrole [20], pyridine [21], and anisole [22], were investigated through experimental, theoretical, and modelling work. These works demonstrated that the respective developed or analysed models could describe the oxidation of small hydrocarbons and tars in reasonable agreement with experimental measurements under oxy-fuel conditions. However, predicting pollutants, such as NO_x and PAHs, remains challenging [8], especially for oxygenated fuels [22–24], nitrogen-containing components [20], or complex mixtures of such species as they emerge from biomass devolatilisation [14].

This section evaluates the progress made in predicting PAHs under oxy-fuel conditions. It is well-established that pollutant formation, especially PAH formation [8,25], is sensitively impacted by fuel-specific chemistry, often making it difficult to identify a single cause for deviations between experimental and computed values. For example, the investigation of atmospheric anisole counterflow diffusion flames [22], discussed in more detail below, showed that tentative updates of the PAH chemistry significantly impacted kinetic model predictions. At the same time, deviations between kinetic model predictions and experimental measurements for important PAH precursors, such as ethylene (C_2H_4), diacetylene (C_4H_2), and vinylacetylene (C_4H_4), could exceed a factor of four [22]. Hence, both uncertainties in the oxidation and the PAH chemistry may significantly contribute to the discrepancies observed for PAH mole fractions.

The analysis of Chen et al. [22] illustrates that identifying causes for unsatisfactory PAH predictions can be challenging if simulations involve novel kinetic models with significant prediction uncertainties for small dehydrogenated intermediates. For the complex composition of volatiles, analysis could additionally be hampered by potential interactions of nitrogen-containing and hydrocarbon species [26]. The approach in the present work alleviates this challenge by exploiting the current understanding that molecular growth pathways are primarily initiated by relatively small dehydrogenated species with up to five carbon (C) atoms [8]. Consequently, PAH formation can be investigated by considering the combustion of small hydrocarbons, which reduces relevant uncertainties in PAH precursor predictions. In addition, the effects of fuel-specific chemistry on the evaluation are reduced by considering several fuels.

Burning solid fuels under oxy-fuel conditions can significantly impact combustion. For equal fractions of O_2, the maximum flame temperatures are substantially lower in oxy-fuel combustion compared to combustion in air, owing to the higher specific heat of CO_2. Excess CO_2 can participate in chemical reactions either as a reactant or as a third body for collision, affecting the fuel consumption and pollutant formation pathways. Cai et al. [15] demonstrated that their previously published detailed chemical kinetic model [27] could reasonably reproduce several measurements obtained for methane (CH_4) combustion under oxy-fuel conditions, including

extinction limits of counterflow flames [15,28–30], ignition delay times [31–33], and laminar flamespeeds [34–38]. The model of Cai et al. [27] also contains detailed PAH chemistry [39] and was extensively validated against various targets relevant to C_0–C_4 chemistry. Therefore, it constitutes a suitable reference point for evaluating the recent progress in modelling PAH predictions under oxy-fuel conditions.

A review of the analyses performed in the above-mentioned studies [15–18,22] suggests that advancements in recently published kinetic modelling work are relevant to predicting PAH formation from oxy-fuel combustion. Langer et al. [8] and Langer [40] developed a detailed chemical kinetic model for PAHs that builds upon the model of Cai et al. [27]. The most recent revision of the model by Hellmuth et al. [41] introduced updates to the C_7H_7 kinetics. This model [41] will be called the "ITV model" in the following. Besides an extensive revision of the PAH chemistry [8,40,41], Langer et al. [8] and Langer [40] introduced several updates to the C_0–C_4 core chemistry that are expected to impact combustion under oxy-fuel conditions. For example, Langer et al. [8] updated the rate coefficient of the reaction $CO + OH = CO_2 + H$ based on the theoretical work of Senosiain et al. [42]. This reaction may be particularly significant under oxy-fuel conditions because it sensitively influences hydrogen (H) radical availability [15], which may strongly affect PAH formation. Further modifications include the integration of the C_3 chemistry from the modelling work of Panigrahy et al. [43]. Baroncelli et al. [16] showed that C_3 chemistry plays a crucial role in aromatics formation from the non-premixed combustion of two of the most abundant devolatilisation products [16], methane and acetylene (C_2H_2). Updates to the PAH chemistry [8] that are expected to be particularly relevant include radical recombination reactions involving five-membered ring species. Reaction flux analysis of Chen et al. [22] for anisole counterflow diffusion flames suggests that introduced updates of the cyclopentadienyl radical self-recombination reactions ($C_5H_5 + C_5H_5$) are critical, as this was found to be the dominant naphthalene (A_2) formation pathway. The ITV model [41] is directly comparable to the model of Cai et al. [27] and was last updated in 2024. Hence, this is another suitable reference point for evaluating recent progress in PAH modelling under oxy-fuel conditions.

Figures 6.1 and 6.2 compare predictions obtained with the model of Cai et al. [27] and the ITV model [41] to measurement data for several fuels. The comparison considers data from time-of-flight mass spectrometry (ToF-MS) [16–18,44–46] and gas chromatography (GC) [41,47,48], including investigations performed within *Oxyflame* [16–18,41]. Figures 6.1 and 6.2 show that deviations between measured and predicted species peak mole fractions decreased for cyclopentadiene (C_5H_6), benzene (A_1), phenylacetylene (A_1C_2H), styrene ($A_1C_2H_3$), ethylbenzene ($A_1C_2H_5$), indene (C_9H_8), naphthalene, and acenaphthylene ($C_{12}H_8$) when comparing the ITV model [41] to the model of Cai et al. [27]. The only exception is toluene (A_1CH_3), although the predictions remain accurate. The computed mean deviation factors [8] shown in the bottom right of the parity diagrams in Figs. 6.1 and 6.2 highlight a considerable improvement for phenylacetylene and acenaphthylene, whose mean deviation factors reduce by more than a factor of four. This

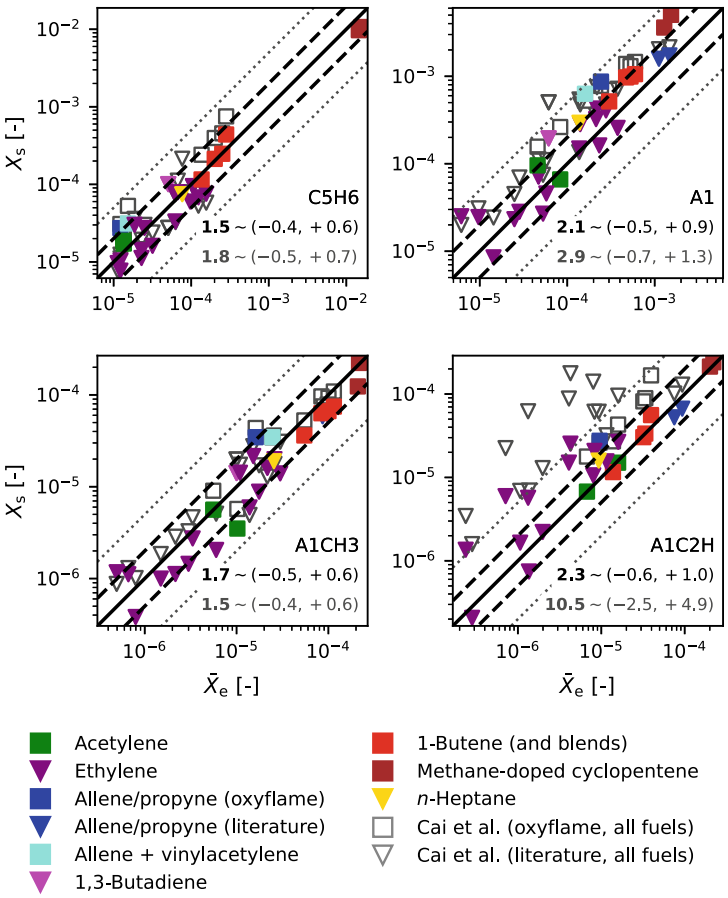

Fig. 6.1 Parity diagrams comparing peak mole fractions from measurements to simulation results. Single species or isomer mole fractions were selected as appropriate for the respective experiment. Dashed lines indicate a deviation of a factor of two, and dotted lines a factor of five. Results obtained with the ITV model [41] use colours representing the fuel composition (acetylene [16], ethylene [47,48], allene or propyne [41,45], allene/vinylacetylene [41], 1,3-butadiene [46], 1-butene or 1-butene blends [18], methane-doped cyclopentene [17], *n*-heptane [44]). Results obtained with the model of Cai et al. [27] are shown as empty symbols. Experimental data measured as a part of *Oxyflame* are shown as squares, and other literature data are shown as triangles. Values in the bottom right are the average deviation factor and estimates of the associated 90 %-confidence intervals [8] for the ITV model [41] (upper row) and the model of Cai et al. [27] (lower row), respectively

quantitative evaluation illustrates that the ITV model [41] is suitable for investigating oxy-fuel combustion and PAH formation. Therefore, it was chosen as the basis for developing a compact model for biomass combustion in the subsequent sections.

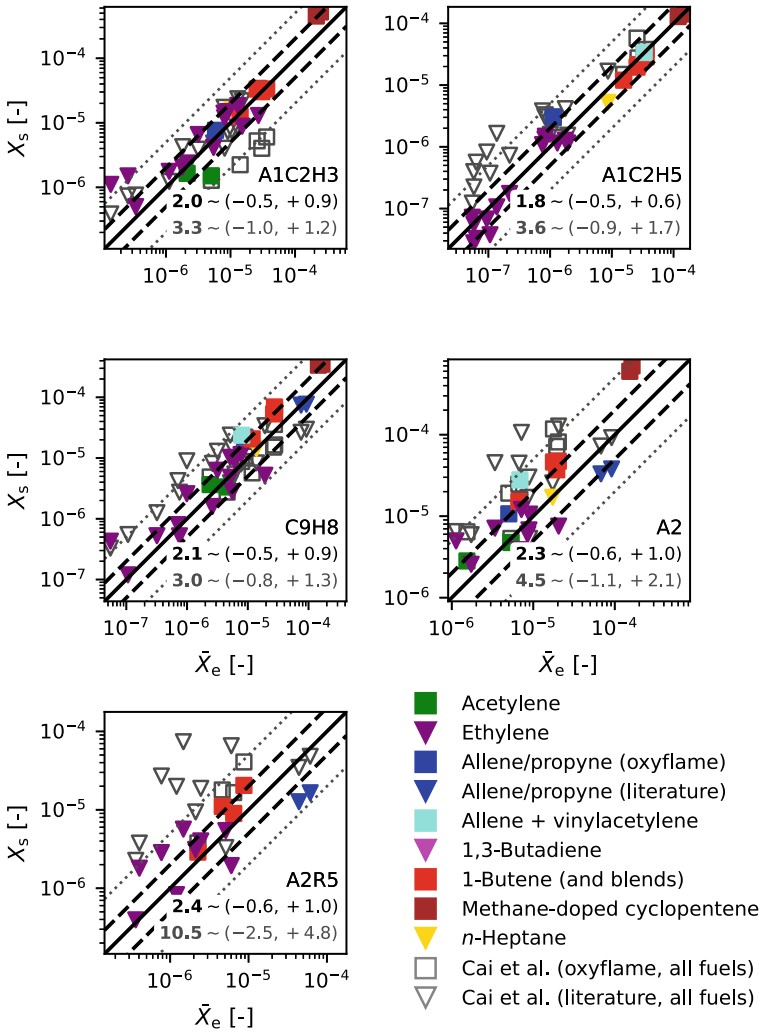

Fig. 6.2 Parity diagrams comparing peak mole fractions from measurements to simulation results. Results obtained with the ITV model [41] use colours representing the fuel composition. Results obtained with the model of Cai et al. [27] are shown as empty symbols. An explanation of the symbol shapes, the lines, and the numbers at the bottom right, as well as references to the experimental data, can be found in the caption of Fig. 6.1

6.3 Skeletal Kinetic Model for Biomass Surrogate Components

Modelling the gas-phase chemistry of biomass fuels requires the description of the underlying chemistry that governs the volatilisation and gas-phase processes. However, a detailed representation of these processes results in complex chemical kinetic models, making their use computationally impractical in large-scale simulations. This section addresses the development of a skeletal, i.e. compact, chemical kinetic model suitable for large-scale simulations, which is based on the ITV model [41] discussed in Sect. 6.2. The skeletal model was specifically designed to predict the gas-phase chemistry of biomass fuels under conditions relevant to practical applications, including high-temperature atmospheric combustion in air or oxy-fuel environments.

Figure 6.3 illustrates the development process.

Developing such a model first requires deriving a surrogate formulation to approximate the volatile mixture composition released from the fuels targeted in the numerical investigation. Here, the particle devolatilisation model proposed by Ranzi et al. [9] and further extended by Debiagi et al. [49] was applied to three different biomass particles: raw miscanthus, torrefied miscanthus, and torrefied corn straw. The particle devolatilisation model provides complex mixtures including light hydrocarbons, oxygenated species, aldehydes, tars, aromatics, and several nitrogen-containing species. The latter includes nitrogen tars and light compounds such as ammonia and hydrogen cyanide. Since the ITV model [41] development did not target biomass fuels, the chemistry of missing volatiles found in significant amounts in the mixture was integrated in this step. Anisole was selected as the primary representative of oxygen-containing tars, levoglucosan ($C_6H_{10}O_5$) as the dominant tar component of cellulose devolatilisation, and propionaldehyde (CH_3CH_2CHO) as the main representative of

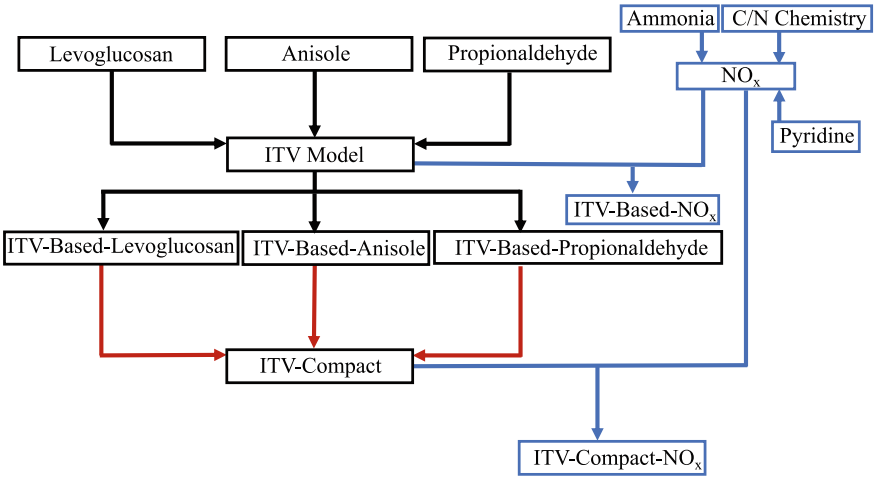

Fig. 6.3 Development process of the compact surrogate model. Black arrows denote the integration of tars surrogate components with the ITV model, red arrows indicate the reduction and merging steps, and blue arrows denote steps related to the development of the skeletal NO_x submodel and its integration with the other models

aldehydes. The work of Debiagi et al. [13], Wagnon et al. [50] and Pelucchi et al. [51] provided the kinetic models for levoglucosan, anisole, and propionaldehyde, respectively. The subchemistry models of the three species were individually integrated with the ITV model, resulting in three models labeled with the prefix "ITV-Based" followed by the name of the integrated volatile (see Fig. 6.3). The ITV-Based models were reduced to a skeletal level and combined into one compact surrogate model, named "ITV-Compact". To include the nitrogen-containing species from the volatile mixture, an additional skeletal NO_x submodel was developed to accurately describe the primary NO_x formation pathways and the oxidation chemistry of pyridine. The latter was selected as a representative species for nitrogen tars. The following sections provide a more detailed description of the ITV-Compact model development steps.

6.3.1 ITV-Compact Model Development

The three detailed ITV-Based models were reduced to a skeletal level using the directed relation graph with error propagation (DRGEP) methodology [52]. The goal of the reduction process was to preserve the accuracy of the detailed models when predicting the oxidation of major volatiles under air and oxy-fuel environments at atmospheric pressure and high temperatures. Ignition delay times were selected as the main combustion characteristic whose accuracy had to be retained during the reduction phase. Experimental data from the literature were used to define model-specific reduction targets, thereby determining the validity range of the skeletal kinetic models. Target species for the reduction procedure included the volatiles of interest (anisole, propionaldehyde, and levoglucosan), major combustion products (carbon monoxide (CO), CO_2, and water (H_2O)), and smaller intermediate species, such as hydrogen (H_2), methane, ethylene, and ethane (C_2H_6). The reduced models were then systematically combined to develop the ITV-Compact surrogate model, which comprises 104 species. The merging process was carried out incrementally, starting with the smallest model and progressively integrating larger ones by identifying and incorporating missing species and corresponding reactions. Two key factors facilitated this merging strategy: First, the reduced models were derived from detailed models that shared the same base chemistry, minimising potential conflicts during merging. Second, the reduction targets for each ITV-Based model included a shared set of conditions to represent the oxidation chemistry of small volatiles, differing exclusively in conditions specific to the oxidation of the integrated volatiles. As a result, consistency was ensured among the core chemistry of the reduced models, and differences were primarily confined to the integrated tar-specific chemistry.

The validation of the ITV-Compact model considered zero- and one-dimensional configurations, including measurements of ignition delay times in shock tubes and species mole fractions in counterflow diffusion flames. Predictions from the ITV-Compact model were compared with those from the corresponding detailed model to quantify reduction effects. Furthermore, comparing the ITV-Based models

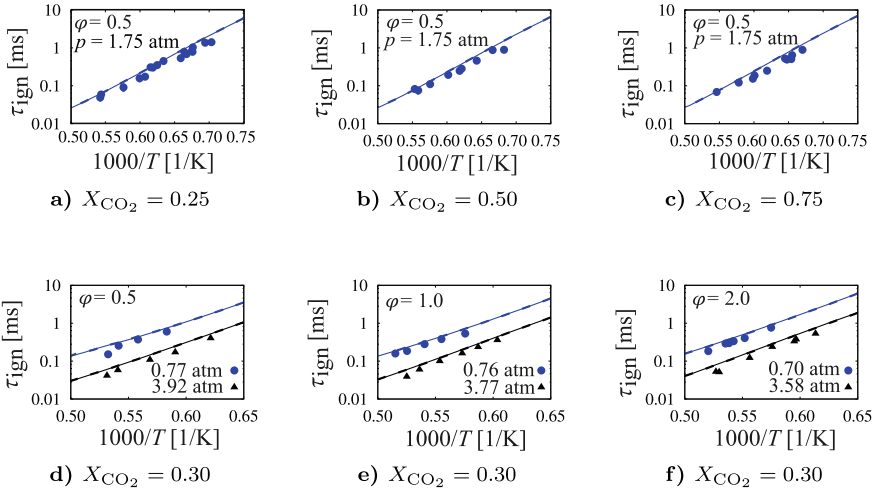

Fig. 6.4 Comparison of ignition delay times of $CH_4/O_2/CO_2$/argon (Ar) mixtures at various pressures (p) and fuel-air equivalence ratios (φ) in a shock tube. Symbols denote the experimental data [31,32], solid lines denote model predictions with the ITV-Compact model, and dashed lines denote the ITV model [41] predictions

to the reference models from which the chemistry of the integrated volatile species was adopted revealed the impact of different base chemistries.

Ignition Delay Times for Small Volatiles

Figures 6.4, 6.5 and 6.6 show measurement results [31,32,53,54] of ignition delay times for small volatiles under oxy-fuel conditions in comparison with model predictions using the ITV-Compact and the ITV model [41]. Notably, the ignition delay times predicted with the ITV model [41] are in good agreement with the experimental data. The minor discrepancies between predictions obtained with ITV-Compact and the ITV model [41] indicate that the reduction process introduced no significant errors in the ignition delay time prediction.

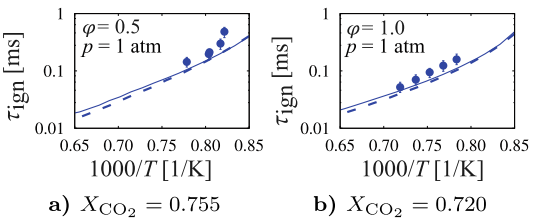

Fig. 6.5 Comparison of ignition delay times of $C_2H_4/O_2/CO_2$ mixtures at lean and stoichiometric conditions in a shock tube. Symbols denote the measurements [53], solid lines denote model predictions with the ITV-Compact model, and dashed lines denote the ITV model [41] predictions

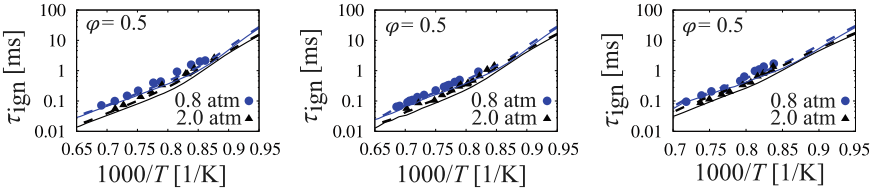

Fig. 6.6 Comparison of ethane ignition delay times of lean $C_2H_6/O_2/CO_2$ mixtures in a shock tube. Symbols denote the measurements [54], solid lines denote model predictions with the ITV-Compact model, and dashed lines denote the ITV model [41] predictions

Propionaldehyde Chemistry

Figure 6.7 displays ignition delay time measurements of Ar/O_2/propionaldehyde mixtures from Pelucchi et al. [51] and Akih-Kumgeh and Bergthorson [55] at three different fuel-air equivalence ratios over a broad range of temperatures. Additionally, predictions with the ITV-Based-Propionaldehyde, the ITV-Compact model, and the model of Pelucchi et al. [51] are shown. The latter functions as a reference model to assess the impact of different base chemistries on propionaldehyde ignition delay times. The ITV-Based-Propionaldehyde model and the model from Pelucchi et al. [51] are in good agreement with the experimental data. Furthermore, only minor discrepancies exist between the ITV-Compact and the ITV-Based-Propionaldehyde model for all validation cases considered in Fig. 6.7.

Anisole Chemistry

Figures 6.8 and 6.9 show experimental speciation profiles of major and intermediate species from the counterflow diffusion flame of Chen et al. [22] with CO_2 as a diluent on the oxidiser side (CO_2O-flame). Additionally, prediction results obtained with the ITV-Based-Anisole, the ITV-Compact model, and the model of Wagnon et al. [50] are presented. The latter was chosen since it provided the anisole-specific chemistry for the ITV-Based models. Predictions obtained with the ITV-Compact

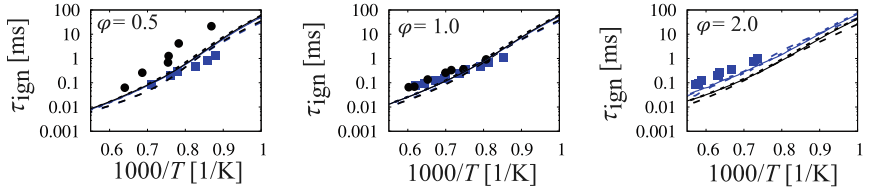

Fig. 6.7 Comparison of measured ignition delay times of Ar/O_2/propionaldehyde mixtures by Pelucchi et al. [51] (blue squares: $p = 1.25$ atm, ($\varphi = 0.5$, $X_{Ar} = 0.91$)/($\varphi = 1.0$, $X_{Ar} = 0.95$)/($\varphi = 2.0$, $X_{Ar} = 0.97$)) and from Akih-Kumgeh and Bergthorson [55] (black circles: atmospheric pressure, ($\varphi = 0.5$, $X_{Ar} = 0.8889$)/($\varphi = 1.0$, $X_{Ar} = 0.939$)/($\varphi = 2.0$, $X_{Ar} = 0.9298$)) to model predictions with the ITV-Compact (solid lines), the ITV-Based-Propionaldehyde model (dotted lines), and the model of Pelucchi et al. [51] (dashed lines). Experimental data from the work of Akih-Kumgeh and Bergthorson [55] were unavailable for the fuel-rich validation case

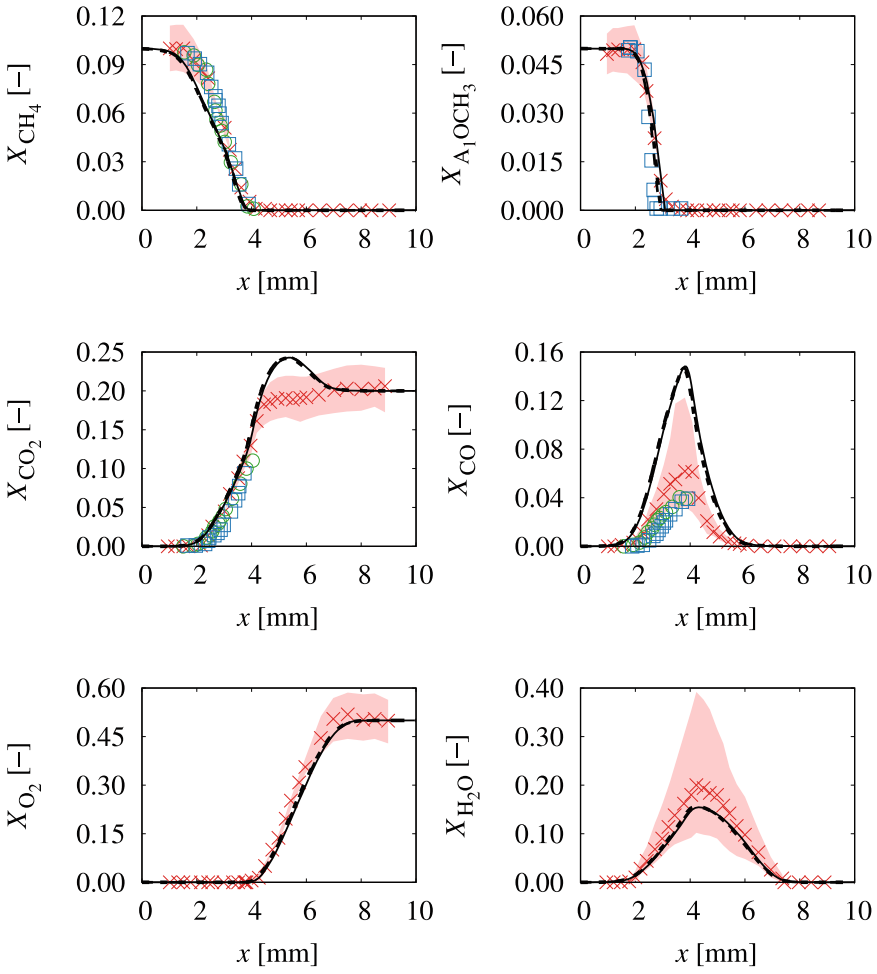

Fig. 6.8 Comparison of measured and predicted mole fractions of reactants and main products for the CO_2O-flame, one of the atmospheric anisole diffusion flames investigated by Chen et al. [22]. Experimental data were obtained using three measurement techniques: ToF-MS (red crosses), GC with a *Restek Rt-Q-Bond* column (blue squares), and GC with an *Agilent DB-Petro* column (green circles). Predictions with the ITV-Compact model, the ITV-Based-Anisole model, and the model of Wagnon et al. [50] are depicted by solid, dotted, and dashed lines. The red-shaded areas indicate the uncertainty in the ToF-MS measurements. The spatial coordinate x refers to the distance from the fuel nozzle

and the ITV-Based-Anisole models show no discernable difference. Moreover, predictions with the ITV-Based-Anisole and the Wagnon et al. [50] models exhibit no discrepancies, indicating that the differences in their base chemistries are negligible.

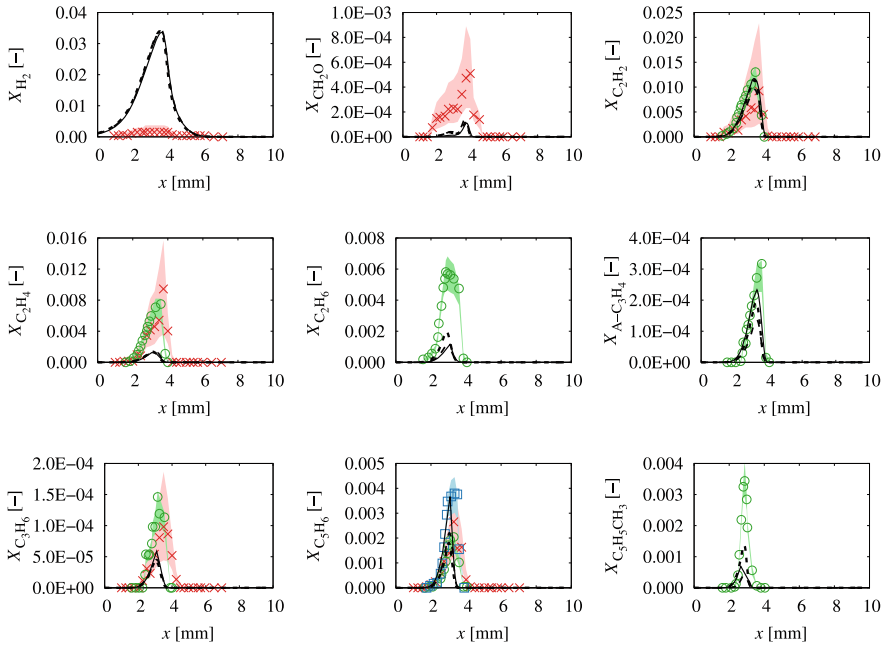

Fig. 6.9 Comparison of experimentally measured and predicted mole fractions of small intermediates and hydrocarbons for the CO_2O-flame, one of the atmospheric anisole diffusion flames investigated by Chen et al. [22]. Experimental data were obtained using three measurement techniques: ToF-MS (red crosses), GC with a *Restek Rt-Q-Bond* column (blue squares), and GC with an *Agilent DB-Petro* column (green circles). Predictions with the ITV-Compact model, the ITV-Based-Anisole model, and the model of Wagnon et al. [50] are depicted by solid, dotted, and dashed lines. Shaded areas with different colours indicate the measurement uncertainty of the respective techniques. The spatial coordinate x refers to the distance from the fuel nozzle

6.3.2 NO_x Submodel

Nitrogen oxides are harmful pollutants that pose significant environmental and health risks. In biomass combustion, fuel-NO_x is the predominant nitric oxide (NO) formation mechanism [7], i.e. NO_x primarily originates from the oxidation of light nitrogen-containing species such as hydrogen cyanide, isocyanic acid (HNCO), and ammonia. These species can be directly released during the devolatilisation of solid particles or formed through tar-nitrogen cracking [6,7]. Therefore, simulations of biomass combustion require, first and foremost, an accurate model of fuel-NO_x formation. In addition to fuel-NO_x pathways, nitrous dioxide (N_2O) chemistry and prompt-NO_x and thermal-NO_x pathways can contribute to overall NO_x emissions and must be included. This section introduces a newly developed NO_x submodel suitable for biomass combustion. As illustrated in Fig. 6.3, the model consists of three subsets: the C-N, ammonia, and tar-nitrogen (represented by pyridine) chemistry. The subsets are discussed in the following. Since this work aims to develop

a NO_x model suitable for large-scale simulations, relevant kinetic mechanisms for the C-N and ammonia chemistry were extracted from the detailed NO_x submodel through systematic reduction using the DRGEP method [52]. The selection of reduction targets for these subsets is also outlined below.

Subset Model Selection and Adaption

The developed model for C-N chemistry is based on the comprehensive review of Glarborg et al. [7]. Subsets were adopted from the model of Glarborg et al. [7] because their choice of rate coefficients and thermochemistry parameters was informed by extensive literature surveys that considered both ab initio calculations and experimental measurements. The adopted subsets include the oxidation kinetics of nitrogen-containing species, such as hydrogen cyanide, isocyanic acid, and prompt-NO_x formation pathways. The model also accounts for interactions between small nitrogen-containing and hydrocarbon species, which is particularly relevant in biomass combustion due to the complex and heterogeneous mixtures of volatiles released during devolatilisation. A subset of the validation data compiled by Glarborg et al. [7] was also used to design the reduction targets for the C-N submodel, focusing on experimental conditions covering the oxidation chemistry of hydrogen cyanide, isocyanic acid, hydrocarbon-nitrogen interactions, and prompt-NO_x formation.

The ammonia model provides a detailed description of ammonia combustion behaviour. It includes the kinetics of the thermal DeNOx process, which plays a crucial role in ammonia oxidation, as well as the N_2O and thermal NO_x formation pathways. Ammonia chemistry was incorporated from the model of Zhang et al. [56]. This choice was based on a quantitative evaluation of twelve chemical kinetic models, which demonstrated that the model of Zhang et al. [56] performed best across a wide range of experimental conditions [57]. The model was systematically reduced to a skeletal level, with reduction targets including ignition delay times at pressures between 1 and 5 bar, temperatures between 1200 and 1600 K, and fuel-air equivalence ratios between 0.5 and 1, and laminar burning velocities at ambient conditions for fuel-air ratios between 0.7 and 1.4. The reduction process was conducted while ensuring that the skeletal kinetic model maintained the same level of performance as the detailed model, as indicated by the mean score [58], quantifying the agreement between experimental data and their computed counterparts.

The reduced model developed by Shamooni et al. [59] provided the pyridine chemistry. Modifications to the C-N chemistry [7] helped to improve the agreement with experimentally measured NO speciation profiles from pyridine oxidation, as shown in Fig. 6.10. Specifically, the frequency factor of the reaction $NCO + NO = N_2O + CO$ was decreased by a factor of two, and the rate parameters of the reaction $NCO + O = NO + CO$ were adopted from Shamooni et al. [59].

The result is a NO_x submodule that consists of 36 species. This makes it well-suited for large-scale simulations, which demand accurate NO_x predictions.

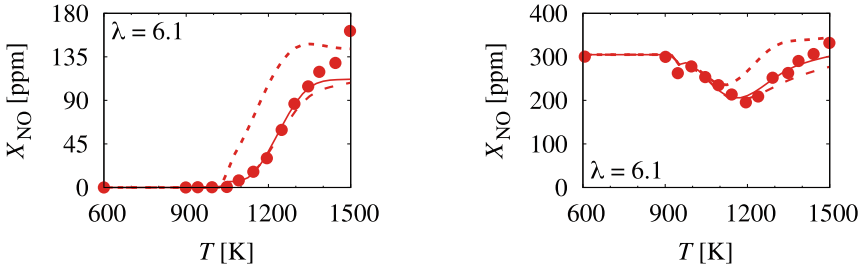

Fig. 6.10 Mole fractions of NO as a function of temperature for atmospheric isothermal pyridine oxidation in a flow reactor at an air-fuel ratio (λ) of 6.1 (set 7 and 8) [60]. The sets differ in their dilution level and initial share of NO. The NO_x submodel predictions are shown with the modified (solid lines) and unchanged (dotted lines) rate parameters for the reactions NCO + NO = N_2O + CO and NCO + O = NO + CO. Dashed lines represent predictions of the model of Shamooni et al. [59], and symbols are experimental data

NO_x Chemistry Validation for the Oxidation of Light Volatiles and Pyridine

Integrating the NO_x submodel with the ITV-Compact and the ITV model [41] resulted in two different models, referred to as the "ITV-Compact-NO_x" and the "ITV-Based-NO_x" model (see Fig. 6.3), respectively. Validation starts by evaluating the ITV-Compact-NO_x model's capability to predict NO_x formation from smaller volatile species, i.e. isocyanic acid (Fig. 6.11), hydrogen cyanide (Fig. 6.12), and ammonia (Fig. 6.13). Figures 6.11–6.13 also include predictions with the ITV-Based-NO_x model to assess the impact of differing base chemistries on NO_x formation pathways. This comparison is particularly relevant for cases with potential interactions between nitrogen-containing species and smaller hydrocarbons. Further, the ITV-Based-NO_x model's performance was evaluated against the performance of the model of Glarborg et al. [7], since it is the reference source for C-N chemistry. Flow reactor measurements [7,61,62] served as validation targets for the oxidation of isocyanic acid (Fig. 6.11) and hydrogen cyanide (Fig. 6.12). The predictions with the ITV-Compact-NO_x and ITV-Based-NO_x models closely align and show only minor discrepancies compared to those with the model of Glarborg et al. [7]. Matching the latter highlights the successful preservation of the predictive accuracy of the C-N chemistry. Similarly, Fig. 6.13 illustrates good agreement between predictions with the ITV-Compact-NO_x and ITV-Based-NO_x models for NO formation from CH_4/NH_3 oxidation at different fuel-air equivalence ratios. Differences in ammonia consumption compared to the model of Glarborg et al. [7] were attributed to variations in the ammonia chemistry.

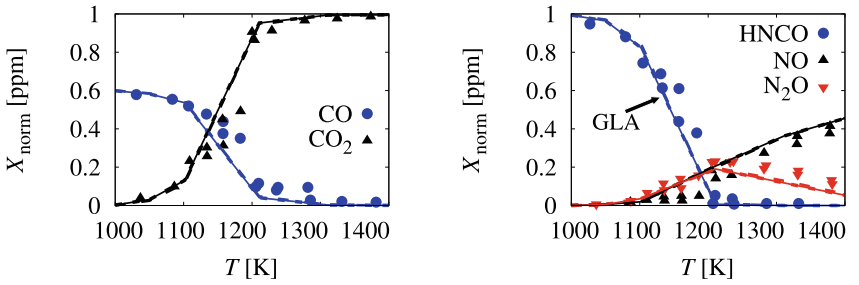

Fig. 6.11 Comparison of flow reactor measurements (symbols) of Glarborg et al. [63] for HNCO oxidation at a pressure of 1.05 atm to predictions with the ITV-Compact-NO_x (solid lines), the ITV-Based-NO_x (dotted lines) models, and the model of Glarborg et al. [7] (dashed lines, GLA). The inlet HNCO mole fraction normalises the shown mole fractions. Inlet mole fractions were HNCO = 480 ppm, CO = 730 ppm, O_2 = 5.5 %, and H_2O = 0.5 %, balanced by nitrogen (N_2)

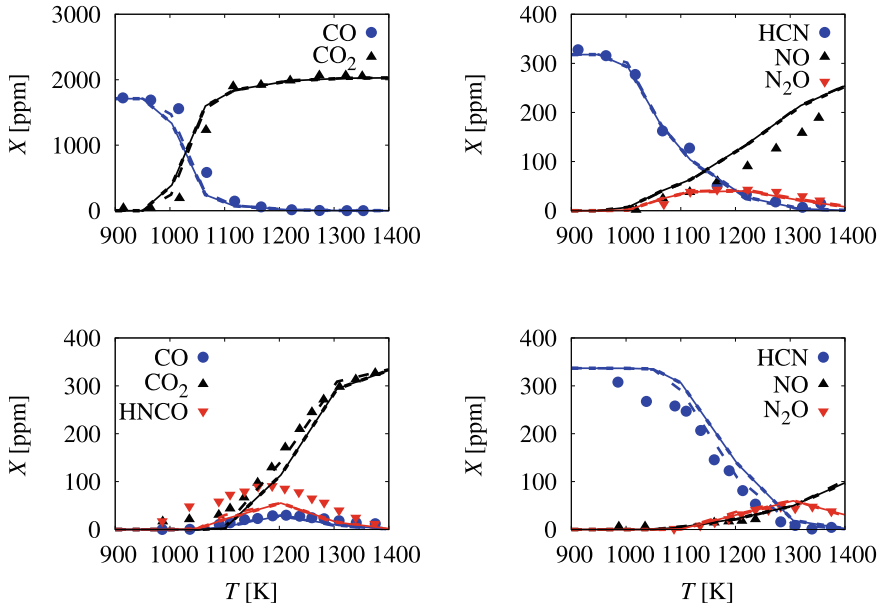

Fig. 6.12 Comparison of flow reactor experimental data (symbols) from Hulgaard and Dam-Johansen [61] and Glarborg and Miller [62] for HCN oxidation at a pressure of 1.05 atm with (upper row, inlet mole fractions were HCN = 318 ppm, CO = 1710 ppm, O_2 = 2.4 %, and H_2O = 2.8 %, balanced by N_2) and without CO in the inlet (lower row, inlet mole fractions were HCN = 337 ppm, O_2 = 2.6 %, and H_2O = 3.1 %, balanced by N_2) against predictions from the ITV-Compact-NO_x (solid lines), the ITV-Based-NO_x (dotted lines) models, and the model of Glarborg et al. [7] (dashed lines)

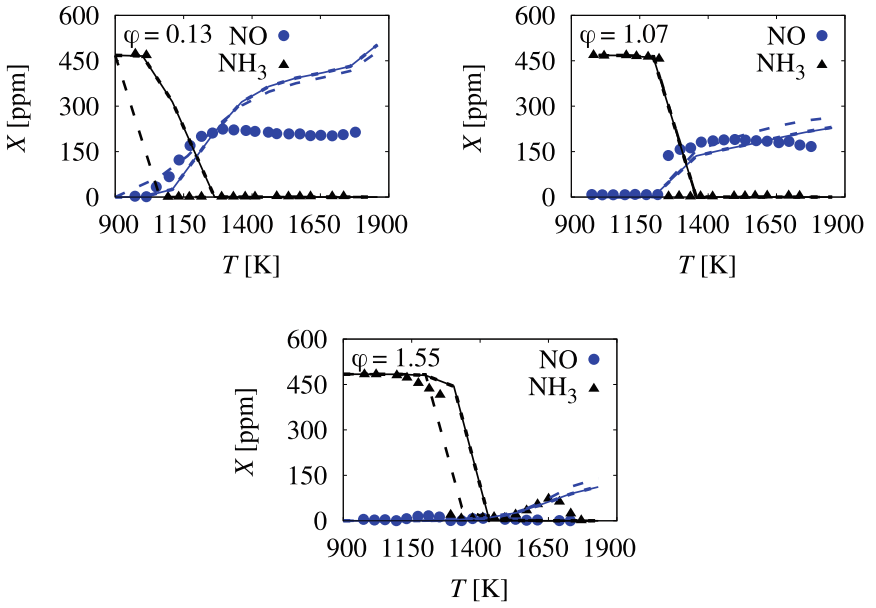

Fig. 6.13 Comparison of atmospheric flow reactor measurements (symbols) of CH_4 and NH_3 of Mendiara and Glarborg [64] at different stoichiometry to predictions with the ITV-Compact-NO_x (solid lines), the ITV-Based-NO_x (dotted lines) models, and the model of Glarborg et al. [7] (dashed lines). Inlet mole fractions for $\varphi = 0.13/1.07/1.55$ were $CH_4 = 2508/2513/2515$ ppm, $O_2 = 3480/5040/40100$ ppm, and $NH_3 = 468/468/484$ ppm, balanced by N_2

The validation of pyridine oxidation in Fig. 6.14 follows the same scheme as for the smaller volatile species, except that the model of Shamooni et al. [59] was considered since it provided the pyridine chemistry. The predictions with the ITV-Compact-NO_x and ITV-Based-NO_x models agree well and differ little from the ones of the model of Shamooni et al. [59], except for the N_2O profiles, for which they show improved prediction accuracy.

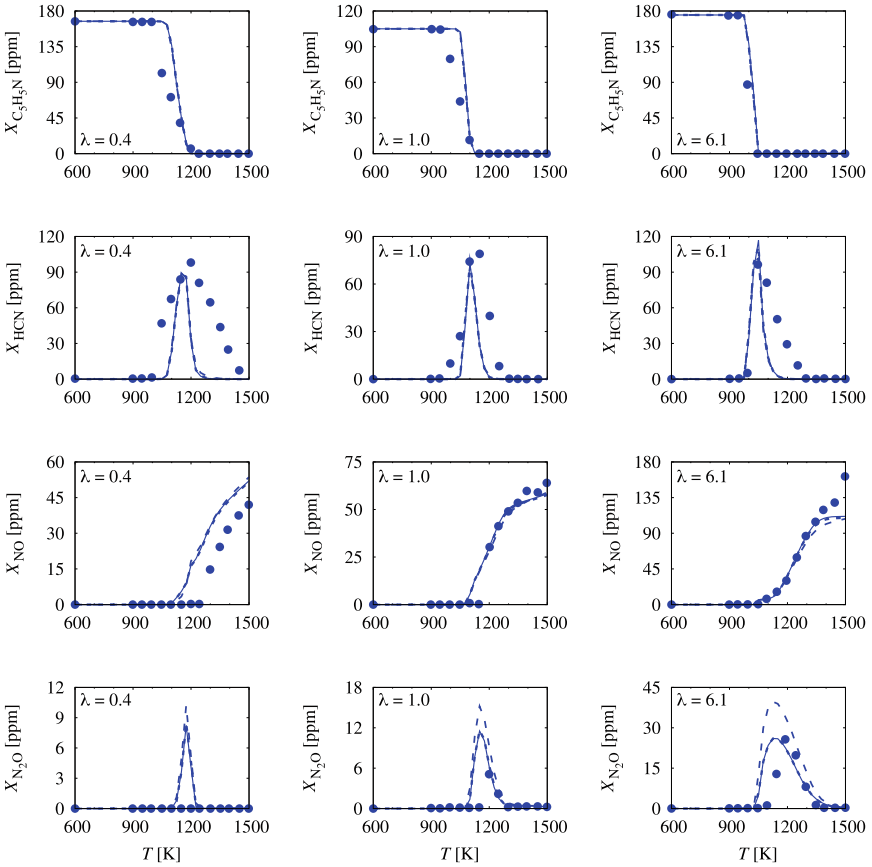

Fig. 6.14 Comparison of atmospheric flow reactor measurements (symbols) of Alzueta et al. [60] to predictions with the ITV-Compact-NO_x (solid lines), the ITV-Based-NO_x (dotted lines) models, and the model of Shamooni et al. [59] (dashed lines). Initial conditions correspond to set 3 ($\lambda = 0.4$), set 5 ($\lambda = 1.0$), and set 7 ($\lambda = 6.1$) Alzueta et al. [60]

6.4 Conclusion

This chapter investigated the gas-phase combustion chemistry of biomass-released volatiles under oxy-fuel conditions and in air. Progress in detailed chemical kinetic modelling of PAH formation from combustion under these conditions was evaluated by comparing predictions of two literature models [27,41]. Both models [27,41] proved suitable for the investigation of combustion under oxy-fuel conditions. However, analyses revealed that the ITV model [41] predicts the mole fractions of aromatic species measured in counterflow flames more accurately than its predecessor [27]. Mean deviations between measured and predicted peak mole fractions of aromatic

species obtained with the ITV model [41] are, on average, close to a factor of two for a broad range of conditions and fuels. The enhanced predictive capabilities and revisions of the C_0–C_4 chemistry make the ITV model [41] the recommended choice for further investigations of oxy-fuel combustion.

Building upon the ITV model [41], a skeletal kinetic model for biomass combustion is developed. First, a particle devolatilisation model [9,49] identified the main volatile species released under conditions representative of practical applications to determine a surrogate formulation. Anisole, levoglucosan, and propionaldehyde emerged as representative biomass surrogate components. The chemistry of these volatiles was incorporated from literature kinetic models into the ITV model [41], yielding three detailed models, one for each component. These models were then reduced to a skeletal level and merged to develop a compact surrogate model with 104 species. To account for nitrogen-containing species released from the volatile mixture, a 36-species skeletal NO_x submodel is developed that combines subset models from different literature works. This submodel accurately captures key NO_x formation pathways and the oxidation of small nitrogen-containing volatiles and tars. All developed models were validated against detailed kinetic models and experimental data, demonstrating their reliability in predicting critical aspects of biomass combustion under conditions relevant to practical applications. The developed NO_x submodel and a further reduced version of the ITV-Compact model were successfully applied in the numerical simulations conducted in Chaps. 19 and 12, demonstrating their prediction accuracy and suitability for large-scale simulations due to their compact size.

Acknowledgements This work has been funded by the Deutsche Forschungsgemeinschaft (DFG, German Research Foundation)—215035359—SFB/TRR 129 'Oxyflame'.

References

1. Williams, A., Jones, J. M., Ma, L. and Pourkashanian, M. "Pollutants from the Combustion of Solid Biomass Fuels". *Progress in Energy and Combustion Science* 38.2 (2012), 113–137. https://doi.org/10.1016/j.pecs.2011.10.001
2. Jenkins, B., Baxter, L. L., Miles Jr., T. and Miles, T. "Combustion Properties of Biomass". *Fuel Processing Technology* 54.1–3 (1998), 17–46. https://doi.org/10.1016/S0378-3820(97)00059-3
3. Hasse, C., Debiagi, P., Wen, X., Hildebrandt, K., Vascellari, M. and Faravelli, T. "Advanced Modeling Approaches for CFD Simulations of Coal Combustion and Gasification". *Progress in Energy and Combustion Science* 86 (2021), 100938. https://doi.org/10.1016/j.pecs.2021.100938
4. Smooke, M. D. "The Computation of Laminar Flames". *Proceedings of the Combustion Institute* 34.1 (2013), 65–98. https://doi.org/10.1016/j.proci.2012.09.005
5. Pielsticker, S., Gövert, B., Kreitzberg, T., Habermehl, M., Hatzfeld, O. and Kneer, R. "Simultaneous Investigation into the Yields of 22 Pyrolysis Gases from Coal and Biomass in a Small-Scale Fluidized Bed Reactor". *Fuel* 190 (2017), 420–434. https://doi.org/10.1016/j.fuel.2016.10.085

6. Glarborg, P., Jensen, A. D. and Johnsson, J. E. "Fuel Nitrogen Conversion in Solid Fuel Fired Systems". *Progress in Energy and Combustion Science* 29.2 (2003), 89–113. https://doi.org/10.1016/S0360-1285(02)00031-X
7. Glarborg, P., Miller, J. A., Ruscic, B. and Klippenstein, S. J. "Modeling Nitrogen Chemistry in Combustion". *Progress in Energy and Combustion Science* 67 (2018), 31–68. https://doi.org/10.1016/j.pecs.2018.01.002
8. Langer, R., Mao, Q. and Pitsch, H. "A Detailed Kinetic Model for Aromatics Formation from Small Hydrocarbon and Gasoline Surrogate Fuel Combustion". *Combustion and Flame* 258 (2023), 112574. https://doi.org/10.1016/j.combustflame.2022.112574
9. Ranzi, E., Cuoci, A., Faravelli, T., Frassoldati, A., Migliavacca, G., Pierucci, S. and Sommariva, S. "Chemical Kinetics of Biomass Pyrolysis". *Energy & Fuels* 22.6 (2008), 4292–4300. https://doi.org/10.1021/ef800551t
10. Hansson, K.-M., Samuelsson, J., Tullin, C. and Åmand, L.-E. "Formation of HNCO, HCN, and NH_3 from the Pyrolysis of Bark and Nitrogen-Containing Model Compounds". *Combustion and Flame* 137.3 (2004), 265–277. https://doi.org/10.1016/j.combustflame.2004.01.005
11. Wanjun, T., Cunxin, W. and Donghua, C. "An Investigation of the Pyrolysis Kinetics of Some Aliphatic Amino Acids". *Journal of Analytical and Applied Pyrolysis* 75.1 (2006), 49–53. https://doi.org/10.1016/j.jaap.2005.04.003
12. Apicella, B., Russo, C., Ciajolo, A., Cortese, L., Cerciello, F., Stanzione, F., Wütscher, A., Muhler, M. and Senneca, O. "High Temperature Pyrolysis of Lignite and Synthetic Carbons". *Fuel* 241 (2019), 264–272. https://doi.org/10.1016/j.fuel.2018.12.065
13. Debiagi, P., Gentile, G., Pelucchi, M., Frassoldati, A., Cuoci, A., Faravelli, T. and Ranzi, E. "Detailed Kinetic Mechanism of Gas-Phase Reactions of Volatiles Released from Biomass Pyrolysis". *Biomass and Bioenergy* 93 (2016), 60–71. https://doi.org/10.1016/j.biombioe.2016.06.015
14. Debiagi, P., Trinchera, M., Frassoldati, A., Faravelli, T., Vinu, R. and Ranzi, E. "Algae Characterization and Multistep Pyrolysis Mechanism". *Journal of Analytical and Applied Pyrolysis* 128 (2017), 423–436. https://doi.org/10.1016/j.jaap.2017.08.007
15. Cai, L., Kruse, S., Felsmann, D. and Pitsch, H. "A Methane Mechanism for Oxy-Fuel Combustion: Extinction Experiments, Model Validation, and Kinetic Analysis". *Flow, Turbulence and Combustion* 106.2 (2021), 499–514. https://doi.org/10.1007/s10494-020-00138-w
16. Baroncelli, M., Felsmann, D., Hansen, N. and Pitsch, H. "Investigating the Effect of Oxy-Fuel Combustion and Light Coal Volatiles Interaction: A Mass Spectrometric Study". *Combustion and Flame* 204 (2019), 320–330. https://doi.org/10.1016/j.combustflame.2019.03.017
17. Baroncelli, M., Mao, Q., Galle, S., Hansen, N. and Pitsch, H. "Role of Ring-Enlargement Reactions in the Formation of Aromatic Hydrocarbons". *Physical Chemistry Chemical Physics* 22.8 (2020), 4699–4714. https://doi.org/10.1039/c9cp05854k
18. Baroncelli, M., Mao, Q., Pitsch, H. and Hansen, N. "Effects of C_1–C_3 Hydrocarbon Blending on Aromatics Formation in 1-Butene Counterflow Flames". *Combustion and Flame* 230 (2021), 111427. https://doi.org/10.1016/j.combustflame.2021.111427
19. Chen, B., Ilies, B. D., Chen, W., Xu, Q., Li, Y., Xing, L., Yang, J., Wei, L., Hansen, N., Pitsch, H., Sarathy, S. M. and Wang, Z. "Exploring Low Temperature Oxidation of 1-Butene in Jet-Stirred Reactors". *Combustion and Flame* 222 (2020), 259–271. https://doi.org/10.1016/j.combustflame.2020.08.051
20. Chen, B., Liu, P., Pelucchi, M., Guidici, C., Maffei, L. P., Faller, S., Xu, Q., Huang, J., Zhang, F., Huang, C., Leonhard, K., Wang, Z., Mehl, M., Roberts, W. L., Faravelli, T. and Pitsch, H. "New Insights into the Oxidation Chemistry of Pyrrole, an N-Containing Biomass Tar Component". *Proceedings of the Combustion Institute* 39.1 (2023), 73–84. https://doi.org/10.1016/j.proci.2022.07.019
21. Chen, B., Lyu, H., Liu, P., Samaras, V. G., Lu, X., Gao, X., Roberts, W. L. and Pitsch, H. "On the Formation of Pyridine, the First Nitrogen Heterocyclic Ring in NPAHs". *Proceedings of the Combustion Institute* 40.1–4 (2024), 105675. https://doi.org/10.1016/j.proci.2024.105675
22. Chen, B., Hellmuth, M., Faller, S., May, L., Liu, P., Cai, L., Roberts, W. L. and Pitsch, H. "Exploring the Combustion Chemistry of Anisole in Laminar Counterflow Diffusion-Flames

Under Oxy-Fuel Conditions". *Combustion and Flame* 243 (2022), 111929. https://doi.org/10.1016/j.combustflame.2021.111929
23. Hellmuth, M., Cameron, F., Faller, S., Schmückert, L., Chen, B., Ren, Y. and Pitsch, H. "Synergistic Effect on PAH and Soot Formation in Ethylene Counterflow Diffusion Flames by the Addition of 1,3-Dioxolane – a Bio-Hybrid Fuel". *Proceedings of the Combustion Institute* 39.1 (2023), 899–908. https://doi.org/10.1016/j.proci.2022.07.164
24. Hellmuth, M., Chen, B., Bariki, C., Cai, L., Cameron, F., Wildenberg, A., Huang, C., Faller, S., Ren, Y., Beeckmann, J., Leonhard, K., Heufer, K. A., Hansen, N. and Pitsch, H. "A Comparative Study on the Combustion Chemistry of Two Bio-Hybrid Fuels: 1,3-Dioxane and 1,3-Dioxolane". *The Journal of Physical Chemistry. A* 127.1 (2023), 286–299. https://doi.org/10.1021/acs.jpca.2c06576
25. Wang, H. "Formation of Nascent Soot and Other Condensed-Phase Materials in Flames". *Proceedings of the Combustion Institute* 33.1 (2011), 41–67. https://doi.org/10.1016/j.proci.2010.09.009
26. Liu, P., Chen, B., Bennett, A., Pitsch, H. and Roberts, W. L. "Probing the Influence of Hydrogen Cyanide on PAH Chemistry". *Proceedings of the Combustion Institute* 39.1 (2023), 1139–1146. https://doi.org/10.1016/j.proci.2022.08.088
27. Cai, L., Ramalingam, A., Minwegen, H., Alexander Heufer, K. and Pitsch, H. "Impact of Exhaust Gas Recirculation on Ignition Delay Times of Gasoline Fuel: An Experimental and Modeling Study". *Proceedings of the Combustion Institute* 37.1 (2019), 639–647. https://doi.org/10.1016/j.proci.2018.05.032
28. Maruta, K., Abe, K., Hasegawa, S., Maruyama, S. and Sato, J. "Extinction Characteristics of CH_4/CO_2 Versus O_2/CO_2 Counterflow Non-Premixed Flames at Elevated Pressures up to 0.7 MPa". *Proceedings of the Combustion Institute* 31.1 (2007), 1223–1230. https://doi.org/10.1016/j.proci.2006.08.013
29. Li, Q., Wang, X., Xin, Y., Zhang, Z., Zhang, Y., Hao, C., Meng, M., Zheng, L. and Zheng, L. "A Unified Intermediate and Mechanism for Soot Combustion on Potassium-Supported Oxides". *Scientific Reports* 4 (2014), 4725. https://doi.org/10.1038/srep04725
30. Kim, T. H., Park, J. W., Park, H. Y., Park, J., Park, J. H. and Lim, I. G. "Chemical and Radiation Effects on Flame Extinction and NO Formation in Oxy-Methane Combustion Diluted with CO_2". *Fuel* 177 (2016), 235–243. https://doi.org/10.1016/j.fuel.2016.03.012
31. Hargis, J. W. and Petersen, E. L. "Methane Ignition in a Shock Tube with High Levels of CO_2 Dilution: Consideration of the Reflected-Shock Bifurcation". *Energy & Fuels* 29.11 (2015), 7712–7726. https://doi.org/10.1021/acs.energyfuels.5b01760
32. Koroglu, B., Pryor, O. M., Lopez, J., Nash, L. and Vasu, S. S. "Shock Tube Ignition Delay Times and Methane Time-Histories Measurements During Excess CO_2 Diluted Oxy-Methane Combustion". *Combustion and Flame* 164 (2016), 152–163. https://doi.org/10.1016/j.combustflame.2015.11.011
33. Pryor, O., Koroglu, B., Barak, S., Lopez, J., Ninnemann, E., Nash, L. and Vasu, S. S. "Ignition Delay Times of High Pressure Oxy-Methane Combustion with High Levels of CO_2 Dilution". *Proceedings of ASME Turbo Expo 2017: Turbomachinery Technical Conference and Exposition GT2017*. Charlotte, North Carolina, USA, 2017.
34. Mazas, A. N., Lacoste, D. A. and Schuller, T. "Experimental and Numerical Investigation on the Laminar Flame Speed of CH_4/O_2 Mixtures Diluted with CO_2 and H_2O". *Proceedings of ASME Turbo Expo 2010: Power for Land, Sea and Air GT2010*. Glasgow, United Kingdom, 2010.
35. Di Benedetto, A., Di Sarli, V., Salzano, E., Cammarota, F. and Russo, G. "Explosion Behavior of $CH_4/O_2/N_2/CO_2$ and $H_2/O_2/N_2/CO_2$ Mixtures". *International Journal of Hydrogen Energy* 34.16 (2009), 6970–6978. https://doi.org/10.1016/j.ijhydene.2009.05.120
36. Ratna Kishore, V., Duhan, N., Ravi, M. R. and Ray, A. "Measurement of Adiabatic Burning Velocity in Natural Gas-Like Mixtures". *Experimental Thermal and Fluid Science* 33.1 (2008), 10–16. https://doi.org/10.1016/j.expthermflusci.2008.06.001

37. Chan, Y. L., Zhu, M. M., Zhang, Z. Z., Liu, P. F. and Zhang, D. K. "The Effect of CO_2 Dilution on the Laminar Burning Velocity of Premixed Methane/Air Flames". *Energy Procedia* 75 (2015), 3048–3053. https://doi.org/10.1016/j.egypro.2015.07.621
38. Persis, S. de, Foucher, F., Pillier, L., Osorio, V. and Gökalp, I. "Effects of O_2 Enrichment and CO_2 Dilution on Laminar Methane Flames". *Energy* 55 (2013), 1055–1066. https://doi.org/10.1016/j.energy.2013.04.041
39. Blanquart, G., Pepiot-Desjardins, P. and Pitsch, H. "Chemical Mechanism for High Temperature Combustion of Engine Relevant Fuels with Emphasis on Soot Precursors". *Combustion and Flame* 156.3 (2009), 588–607. https://doi.org/10.1016/j.combustflame.2008.12.007
40. Langer, R. T. "Adjoint Sensitivity Analysis for Chemical Kinetic Model Development". PhD thesis. RWTH Aachen University, 2023. https://doi.org/10.18154/RWTH-2023-06993
41. Hellmuth, M., Langer, R., Meraviglia, A., Beeckmann, J. and Pitsch, H. "The Role of C_3 and C_4 Species in Forming Naphthalene in Counterflow Diffusion Flames". *Proceedings of the Combustion Institute* 40.1–4 (2024), 105620. https://doi.org/10.1016/j.proci.2024.105620
42. Senosiain, J. P., Klippenstein, S. J. and Miller, J. A. "A Complete Statistical Analysis of the Reaction Between OH and CO". *Proceedings of the Combustion Institute* 30.1 (2005), 945–953. https://doi.org/10.1016/j.proci.2004.07.009
43. Panigrahy, S., Liang, J., Ghosh, M. K., Wang, Q.-D., Zuo, Z., Nagaraja, S., Mohamed, A. A. E.-S., Kim, G., Vasu, S. S. and Curran, H. J. "An Experimental and Detailed Kinetic Modeling Study of the Pyrolysis and Oxidation of Allene and Propyne Over a Wide Range of Conditions". *Combustion and Flame* 233 (2021), 111578. https://doi.org/10.1016/j.combustflame.2021.111578
44. Wullenkord, J., Graf, I., Baroncelli, M., Felsmann, D., Cai, L., Pitsch, H. and Kohse-Höinghaus, K. "Laminar Premixed and Non-Premixed Flame Investigation on the Influence of Dimethyl Ether Addition on *n*-Heptane Combustion". *Combustion and Flame* 212 (2020), 323–336. https://doi.org/10.1016/j.combustflame.2019.11.012
45. Kukkadapu, G., Wagnon, S. W., Pitz, W. J. and Hansen, N. "Identification of the Molecular-Weight Growth Reaction Network in Counterflow Flames of the C_3H_4 Isomers Allene and Propyne". *Proceedings of the Combustion Institute* 38.1 (2021), 1477–1485. https://doi.org/10.1016/j.proci.2020.07.130
46. Moshammer, K., Seidel, L., Wang, Y., Selim, H., Sarathy, S. M., Mauss, F. and Hansen, N. "Aromatic Ring Formation in Opposed-Flow Diffusive 1,3-Butadiene Flames". *Proceedings of the Combustion Institute* 36.1 (2017), 947–955. https://doi.org/10.1016/j.proci.2016.09.010
47. Figura, L. and Gomez, A. "Structure of Incipiently Sooting Ethylene-Nitrogen Counterflow Diffusion Flames at High Pressures". *Combustion and Flame* 161.6 (2014), 1587–1603. https://doi.org/10.1016/j.combustflame.2013.11.023
48. Carbone, F., Gleason, K. and Gomez, A. "Pressure Effects on Incipiently Sooting Partially Premixed Counterflow Flames of Ethylene". *Proceedings of the Combustion Institute* 36.1 (2017), 1395–1402. https://doi.org/10.1016/j.proci.2016.07.041
49. Debiagi, P., Pecchi, C., Gentile, G., Frassoldati, A., Cuoci, A., Faravelli, T. and Ranzi, E. "Extractives Extend the Applicability of Multistep Kinetic Scheme of Biomass Pyrolysis". *Energy & Fuels* 29.10 (2015), 6544–6555. https://doi.org/10.1021/acs.energyfuels.5b01753
50. Wagnon, S. W., Thion, S., Nilsson, E. J. K., Mehl, M., Serinyel, Z., Zhang, K., Dagaut, P., Konnov, A. A., Dayma, G. and Pitz, W. J. "Experimental and Modeling Studies of a Biofuel Surrogate Compound: Laminar Burning Velocities and Jet-Stirred Reactor Measurements of Anisole". *Combustion and Flame* 189 (2018), 325–336. https://doi.org/10.1016/j.combustflame.2017.10.020
51. Pelucchi, M., Somers, K. P., Yasunaga, K., Burke, U., Frassoldati, A., Ranzi, E., Curran, H. J. and Faravelli, T. "An Experimental and Kinetic Modeling Study of the Pyrolysis and Oxidation of *n*-C_3–C_5–Aldehydes in Shock Tubes". *Combustion and Flame* 162.2 (2015), 265–286. https://doi.org/10.1016/j.combustflame.2014.07.027

52. Pepiot-Desjardins, P. and Pitsch, H. "An Efficient Error-Propagation-Based Reduction Method for Large Chemical Kinetic Mechanisms". *Combustion and Flame* 154.1–2 (2008), 67–81. https://doi.org/10.1016/j.combustflame.2007.10.020
53. Peng, C., Zou, C., Ren, J., Lin, Q., Xia, W., Luo, J. and Xiao, Y. "Ignition Delay Times of C_2H_4, C_2H_4/*n*-C_4H_{10}, and *n*-C_4H_{10}/*i*-C_4H_{10} Under O_2/CO_2 Atmospheres: Shock Tube Experiments and Kinetic Model". *Combustion and Flame* 254 (2023), 112825. https://doi.org/10.1016/j.combustflame.2023.112825
54. Liu, P., Chen, B., Li, Z., Bennett, A., Sioud, S., Sarathy, S. M. and Roberts, W. L. "Evolution of Oxygenated Polycyclic Aromatic Hydrocarbon Chemistry at Flame Temperatures". *Combustion and Flame* 209 (2019), 441–451. https://doi.org/10.1016/j.combustflame.2019.08.018
55. Akih-Kumgeh, B. and Bergthorson, J. M. "Ignition of C_3 Oxygenated Hydrocarbons and Chemical Kinetic Modeling of Propanal Oxidation". *Combustion and Flame* 158.10 (2011), 1877–1889. https://doi.org/10.1016/j.combustflame.2011.02.015
56. Zhang, X., Moosakutty, S. P., Rajan, R. P., Younes, M. and Sarathy, S. M. "Combustion Chemistry of Ammonia/Hydrogen Mixtures: Jet-Stirred Reactor Measurements and Comprehensive Kinetic Modeling". *Combustion and Flame* 234 (2021), 111653. https://doi.org/10.1016/j.combustflame.2021.111653
57. Girhe, S., Snackers, A., Lehmann, T., Loffredo, F., Glaznev, R., Beeckmann, J. and Pitsch, H. "Ammonia/Hydrogen Combustion: Comprehensive Quantitative Evaluation of Chemical Kinetic Mechanisms and Improvement". 11^{th} *European Combustion Meeting*. Rouen, France, 2023.
58. Olm, C., Zsély, I. G., Pálvölgyi, R., Varga, T., Nagy, T., Curran, H. J. and Turányi, T. "Comparison of the Performance of Several Recent Hydrogen Combustion Mechanisms". *Combustion and Flame* 161.9 (2014), 2219–2234. https://doi.org/10.1016/j.combustflame.2014.03.006
59. Shamooni, A., Debiagi, P., Wang, B., Luu, T. D., Stein, O. T., Kronenburg, A., Bagheri, G., Stagni, A., Frassoldati, A., Faravelli, T., Kempf, A. M., Wen, X. and Hasse, C. "Carrier-Phase DNS of Detailed NO_x Formation in Early-Stage Pulverized Coal Combustion with Fuel-Bound Nitrogen". *Fuel* 291 (2021). https://doi.org/10.1016/j.fuel.2020.119998
60. Alzueta, M. U., Tena, A. and Bilbao, R. "Pyridine Conversion in a Flow Reactor and its Interaction with Nitric Oxide". *Combustion Science and Technology* 174.10 (2002), 151–169. https://doi.org/10.1080/00102200290021470
61. Hulgaard, T. and Dam–Johansen, K. "Homogeneous Nitrous Oxide Formation and Destruction Under Combustion Conditions". *AIChE Journal* 39.8 (1993), 1342–1354. https://doi.org/10.1002/aic.690390811
62. Glarborg, P. and Miller, J. A. "Mechanism and Modeling of Hydrogen Cyanide Oxidation in a Flow Reactor". *Combustion and Flame* 99.3–4 (1994), 475–483. https://doi.org/10.1016/0010-2180(94)90039-6
63. Glarborg, P., Kristensen, P. G., Jensen, S. H. and Dam-Johansen, K. "A Flow Reactor Study of HNCO Oxidation Chemistry". *Combustion and Flame* 98.3 (1994), 241–258. https://doi.org/10.1016/0010-2180(94)90239-9
64. Mendiara, T. and Glarborg, P. "Ammonia Chemistry in Oxy-Fuel Combustion of Methane". *Combustion and Flame* 156.10 (2009), 1937–1949.https://doi.org/10.1016/j.combustflame.2009.07.006